PET Imaging of Tenascin-C with a Radiolabeled Single-Stranded DNA Aptamer

Orit Jacobson*[1], Xuefeng Yan*[1,2], Gang Niu[1], Ido D. Weiss[3], Ying Ma[1], Lawrence P. Szajek[4], Baozhong Shen[2], Dale O. Kiesewetter[1], and Xiaoyuan Chen[1]

[1]Laboratory of Molecular Imaging and Nanomedicine, National Institute of Biomedical Imaging and Bioengineering, National Institutes of Health, Bethesda, Maryland; [2]Department of Radiology, The Fourth Hospital of Harbin Medical University, Harbin, Heilongjiang, China; [3]Laboratory of Molecular Immunology, National Institute of Allergy and Infectious Diseases (NIAID), National Institutes of Health, Bethesda, Maryland; and [4]Positron Emission Tomography Department, Warren Grant Magnuson Clinical Center (CC), National Institutes of Health, Bethesda, Maryland

Tenascin-C is an extracellular matrix glycoprotein that is expressed by injured tissues and by various cancers. Recent publications showed that tenascin-C expression by cancer lesions predicts tumor growth, metastasis, and angiogenesis, suggesting tenascin-C as a potential therapeutic target. Currently there is no noninvasive method to determine tumoral tenascin-C expression in vivo. To address the need for an agent to image and quantify tenascin-C, we report the development of a radioactive PET tracer based on a tenascin-C–specific single-stranded DNA aptamer (tenascin-C aptamer). **Methods:** Tenascin-C aptamer was radiolabeled with ^{18}F and ^{64}Cu. PET imaging studies for the evaluation of tumor uptake and pharmacokinetics of tenascin-C aptamer were performed in comparison to a nonspecific scrambled aptamer (Sc aptamer). **Results:** The labeled tenascin-C aptamer provided clear visualization of tenascin-C–positive but not tenascin-C–negative tumors. The uptake of tenascin-C aptamer was significantly higher than that of Sc aptamer in tenascin-C–positive tumors. The labeled tenascin-C aptamer had fast clearance from the blood and other nonspecific organs through the kidneys, resulting in high tumor contrast. **Conclusion:** Our data suggest that suitably labeled tenascin-C aptamer can be used as a PET tracer to image tumor expression of tenascin-C with a high tumor-to-background ratio and might provide insightful and personalized medical data that will help determine appropriate treatment and monitoring.

Key Words: DNA aptamer; tenascin-C; PET

J Nucl Med 2015; 56:616–621
DOI: 10.2967/jnumed.114.149484

Tenascin-C is an extracellular matrix glycoprotein that is minimally expressed in healthy adult tissue, transiently expressed during injury and tissue remodeling, and downregulated after tissue repair (*1–6*). During malignant transformations of various cancers, the regulation of tenascin-C expression is absent. The protein is highly expressed in neovasculature and tumor stroma, and the presence of tenascin-C was suggested to play a key role in tumor initiation and progression (*3,7–9*).

Tenascin-C expression was shown to contribute to the supportive tumor microenvironment by direct interactions with cells and growth factors and enhancing cell survival, migration, proliferation, and transdifferentiation of tumor cells (*5*). Its expression also affects the tumor tissue by increasing tumor growth, metastasis, angiogenesis, and inhibition of immune surveillance (*4,8,10*). The quantification of tenascin-C expression by various tumors has not been evaluated in human patients because of the lack of a method to quantify the protein noninvasively. Knowledge of tenascin-C concentration could be useful for cancer diagnosis and prediction of tumor responses to therapies (including experimental therapies targeting tenascin-C).

The tumor-supporting role of tenascin-C along with its high expression make tenascin-C a good therapeutic target, and several therapies targeting tenascin-C are being developed for clinical trials (*11–14*). One such example is a modified RNA aptamer (TTA1) that has entered clinical trials in Europe for tumor stromal tenascin-C expression (*15,16*).

Aptamers are short single-stranded oligonucleotides that display high affinity and selectivity for a given target. Aptamers contain unique features such as low immunogenicity, amenability to chemical modification and bioconjugation, and favorable pharmacokinetics, which include rapid blood clearance and tumor penetration (*17,18*). Aptamers are highly specific and selective to their targets and have superior target-to-noise ratios at early time points (*19*). We hypothesized that this characteristic of DNA aptamers is beneficial for imaging purposes, because any aptamer that does not bind to its target will be rapidly cleared.

In this work, we radiolabeled a single-stranded DNA (ssDNA) aptamer, containing 70 nucleotides, that is identified by systematic evolution of ligands by exponential enrichment to target tenascin-C (*20*). Tenascin-C–specific aptamer (tenascin-C aptamer) was compared with a scrambled sequence aptamer (Sc aptamer) that was predicted to have a different secondary structure (Fig. 1) (*21*). The aptamer was labeled with ^{18}F and ^{64}Cu and evaluated for PET imaging of tumor tenascin-C expression.

MATERIALS AND METHODS

General

S-2-(4-isothiocyanate benzyl)-1,4,7-triazacyclononane-1,4,7-triacetic acid (*p*-SCN-Bn-NOTA) was purchased from Macrocyclics. All other solvents and chemicals were purchased from Sigma-Aldrich. ^{18}F-fluoride and ^{64}Cu were obtained from the National Institutes of Health (NIH)

Received Oct. 3, 2014; revision accepted Jan. 19, 2015.
For correspondence or reprints contact: Xiaoyuan Chen, National Institutes of Health, 35A Convent Dr., 35/GD937, Bethesda, MD 20892-3759.
E-mail: shawn.chen@nih.gov
*Contributed equally to this work.
Published online Feb. 19, 2015.

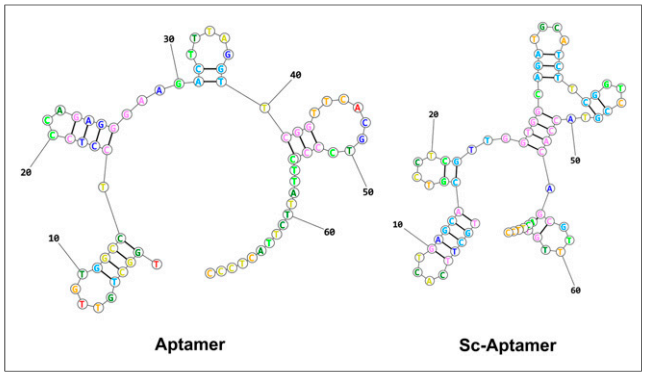

FIGURE 1. Prediction of aptamer secondary structures based on lowest free energy structure.

Clinical Center cyclotron facility. Aptamers and fluorescein isothiocyanate (FITC) aptamers were purchased from Integrated DNA Technologies Inc. The tenascin-C aptamer sequence was 5AmMC6/TGGCTGTTGTGGCCTCCTCCCAGAGGGAAGACTTTAGGTTCGGTTCACGTCCCGCTTATTCTTACTCCC, and the nonspecific Sc aptamer sequence was 5AmMC6/TGCTTCACTGAGCACGTCCTCGTTGGTGGCAGATGCATCTTCGGTCCGTACCACAG CGTTTGTACTTCC. The secondary structure of each aptamer was calculated on the basis of the lowest free energy structure, using RNA structure web servers (*21*).

NAP-5 columns (GE Healthcare Life Sciences) were prewashed before use with 10 mL of water (18.2Ω; Millipore). The concentration of ssDNA aptamers was determined by measuring ultraviolet absorbance at 260 nm on a NanoDrop spectrophotometer (ND-1100; Grace Scientific). Radio–thin-layer chromatography (radio-TLC) was performed on an AR-2000 Bioscan scanner, using 2 systems: instant TLC plates (Agilent) and 0.1 M of citric acid as a developing solvent and reversed-phase C_{18} plates (KC18F, 6 nm [60 Å], 200 mm; Whatman) and 35% CH_3CN:65% 0.1 M triethylamine acetate (pH 7) in water as a solvent. High-performance liquid chromatography (HPLC) was conducted on a system with a variable-wavelength detector operating at 260 nm and with a radioactivity detector containing a NaI crystal. A Phenomenex Luna C_{18} analytic column (5 μm, 4.6 × 250 mm) was used, and the flow was set at 1 mL/min using a slow gradient system, starting from 90% of solvent A (0.1 M triethylamine acetate in water) and 10% of solvent B (CH_3CN) and changing to 70% solvent A and 30% solvent B at 35 min. The conjugation of aptamers with unlabeled *N*-succinimidyl 4-fluorobenzoate (SFB) and *p*-SCN-Bn-NOTA is described in the supplemental materials (available at http://jnm.snmjournals.org).

Mice were purchased from Harlan Laboratories. Female athymic nude mice were housed in an animal facility under pathogen-free conditions. In vivo studies were conducted under protocols approved by the NIH Clinical Center Animal Care and Use Committee and in accordance with the NIH *Guide for the Care and Use of Laboratory Animals* (*22*).

Radiochemistry

Radiosynthesis of ^{18}F-Fluorobenzoyl (FB) Aptamer. The radiosynthesis of ^{18}F-SFB was done as previously reported by us (*23*). ^{18}F-SFB (1.48–2.22 GBq [40–60 mCi]) was redissolved in 20 μL of dimethylformamide. Aptamer (4–10 nmol) dissolved in 50 μL of water was added to the ^{18}F-SFB tube, followed by 180 μL of $Na_2HPO_4 \cdot 7H_2O$ (pH 8.5). The reaction was incubated at 37°C for 30 min. The formation of ^{18}F-FB aptamer was monitored by HPLC. The crude solution of ^{18}F-FB aptamer was loaded onto a NAP-5 column and eluted in 0.25-mL fractions of water. Fraction 4 was the most concentrated, containing 75%–80% of the DNA mass. Fraction 5 was the second most concentrated. Both fractions were used for the biologic studies. HPLC analysis of the 2 fractions showed a similar radiochemical purity of greater than 95%, with a retention time of 17.17 min for FB aptamer and 17.34 min for ^{18}F-FB aptamer. The radiochemical yield of ^{18}F-FB aptamer contained in fractions 4 and 5 was calculated on the basis of ^{18}F-SFB conjugation and non–decay-corrected. The total synthetic procedure beginning with ^{18}F-fluoride required about 2.5 h.

Radiosynthesis of ^{64}Cu-NOTA Aptamer. $^{64}CuCl_2$ (10 μL) was added to 500 μL of 0.4 M ammonium acetate (pH 5.5) to obtain ^{64}Cu-acetate solution. About 10 nmol of NOTA-conjugated aptamer in 20–30 μL of water were added to 100 μL of NH_4OAc buffer. Then 370–444 MBq (10–12 mCi) of ^{64}Cu-acetate (20 μL) were added to give a total volume of 150 μL. The reaction was stirred for 30 min at 37°C. Complexation of ^{64}Cu with the conjugated aptamer was monitored by radio-TLC using system 1 (R_f for ^{64}Cu-NOTA-tenascin-C aptamer = 0.1 and for free ^{64}Cu = 0.9). The reaction was diluted with an additional 100 μL of water and loaded on a NAP-5 column. Labeled aptamer was eluted with water as described above. ^{64}Cu-NOTA aptamers were achieved with a total radiosynthesis time of 50 min and a radiochemical purity greater than 95%.

Biology

^{64}Cu-NOTA Aptamer Analysis In Vitro and In Vivo. Aptamers (1 μg/μL) were incubated in 100 μL of mouse serum (Sigma-Aldrich) or phosphate-buffered saline (PBS) for 1 h at 37°C. Serum has ultraviolet absorbance when loaded on agarose gel, hence the samples incubated in serum were diluted 1:1 in PBS, heated to 95°C for 5 min, and then centrifuged at 13,000*g* for 10 min. The supernatants and the samples in PBS were run on a 2.5% agarose gel (Fisher Scientific). Gel was imaged after staining with GelStar (Lonza) using a Fluorchem camera (α Innotech). ^{64}Cu-NOTA aptamer (3.7–5.5 MBq [100–150 μCi]) was injected into each mouse. For blood analysis, at 30 min and 1 and 2 h after injection, the mice were sacrificed and blood was collected. Urine was collected at the same time points just before the mice were sacrificed. The collected whole blood was allowed to clot for 30–40 min at room temperature. The clot was removed by centrifuging at 3,500 rpm for

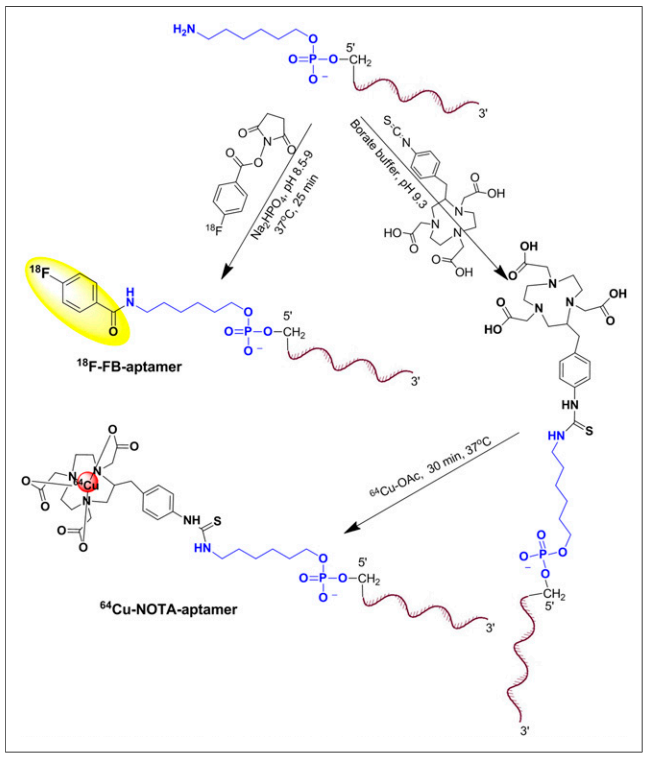

FIGURE 2. ^{18}F and ^{64}Cu aptamer labeling routes.

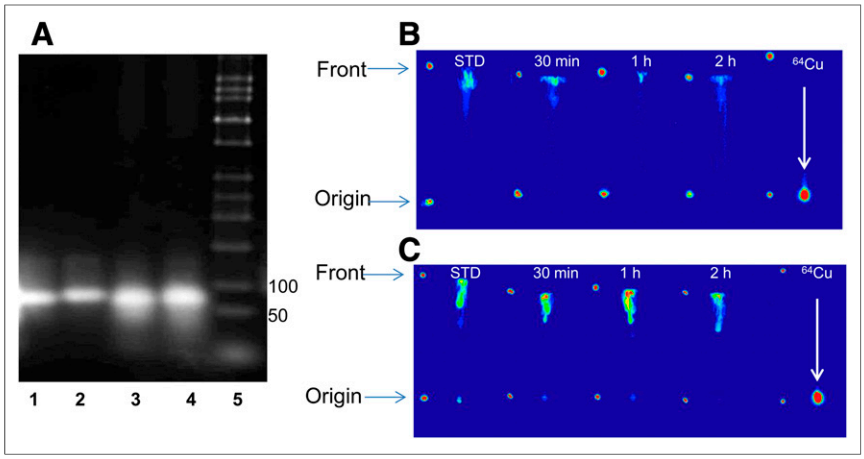

FIGURE 3. (A) Representative agarose gel electrophoresis of tenascin-C aptamer in PBS (1) and postserum incubation (2), Sc aptamer in PBS (3), postserum incubation (4) and ladder (5). (B and C) Representative radio-TLC analysis (autoradiography detection) of ^{64}Cu-NOTA-tenascin-C aptamer of extracts from blood (B) and urine (C) using TLC system 2. R_f for ^{64}Cu-NOTA-tenascin-C aptamer was 0.9 and for free ^{64}Cu it was 0.1 at 30 min and 1 and 2 h after injection of ^{64}Cu-NOTA-tenascin-C aptamer into mice. Blood and urine aliquots were compared with free ^{64}Cu solution loaded as reference (right).

5 min to give the serum. An aliquot of each sample was loaded onto C-18 reversed-phase TLC plates using system 2. The plates were dried and exposed to a phosphor plate (Fuji) for visualization of radioactive bands. The plates were scanned using the Fuji BAS (510 version) scanner.

Cell Culture and Tumor Models. U87MG cells were grown in minimum essential medium (Invitrogen). H460 cells were grown in RPMI-1640 medium (Invitrogen). MDA-MB-435 cells were grown in L-15 medium (Invitrogen). All cell culture media were supplemented with 10% fetal bovine serum (Gibco), 1 mM sodium pyruvate, 2 mM L-glutamine, and nonessential amino acids (Gibco). All cells were grown at 37°C in a humidified atmosphere containing 5% CO_2. Mice were inoculated subcutaneously with 5×10^6 of either U87MG or H460 cells on the right shoulder. The MDA-MB-435 tumor model was generated by orthotopic injection of 5×10^6 cells in the left mammary fat pad of each mouse. The tumors were allowed to develop for 3 wk before imaging studies. Tumor growth was monitored by caliper measurement.

Immunofluorescence Staining. Excised frozen tumor tissue slices (5 μm) were fixed with cold acetone for 20 min and air-dried for 30 min at room temperature. After being blocked with 2% bovine serum albumin for 30 min, the sections were incubated either with rat anti–tenascin-C (1:100; Abcam) for 1 h at room temperature and then visualized with dye-conjugated secondary antibodies (1:200; Jackson Immuno Research Laboratories) or with FITC-labeled tenascin-C aptamer (IDT). After being washed for 35 min with PBS, the whole slides were mounted with 4′,6-diamidino-2-phenylindole–containing mounting medium. Fluorescence images were acquired with an epifluorescence microscope (200X; Olympus, X81).

PET Studies. Tumor-bearing mice were anesthetized using isoflurane/O_2 (1.5%–2% v/v) and injected with 2.96–3.7 MBq (80–100 μCi) of ^{18}F-FB aptamer or ^{64}Cu-NOTA aptamer, in a volume of 100 μL of PBS. PET scans were obtained using an Inveon DPET scanner (Siemens Medical Solutions) at 30 min and 1 and 2 h for ^{18}F-FB aptamer and at 1, 2, 6, and 24 h for ^{64}Cu-NOTA aptamer. PET images were reconstructed without correction for attenuation or scatter using a 3-dimensional ordered-subsets expectation maximization algorithm. ASI Pro VM software (Siemens) was used for image analysis. Regions of interest were drawn for each organ on the coronal images to calculate percentage injected dose per gram (%ID/g), assuming a density of 1 for all tissues.

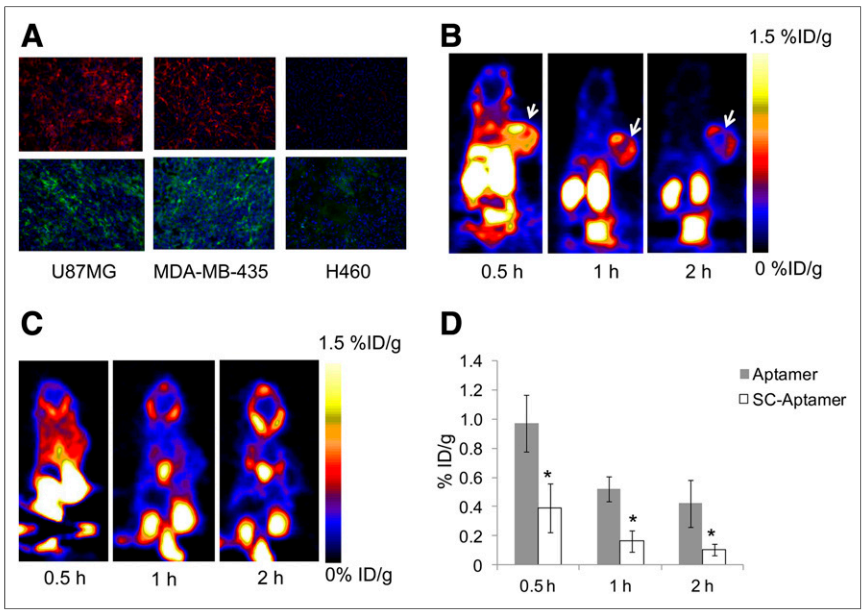

FIGURE 4. (A) Immunofluorescence staining of tenascin-C in frozen section slides of tenascin-C–positive xenografts U87MG and MDA-MB-435 and tenascin-C–negative xenograft H460 using anti–tenascin-C antibody (upper) and FITC-labeled tenascin-C aptamer (lower). Magnification, ×200. (B) Representative coronal PET images of mice bearing subcutaneous U87MG xenograft injected with ^{18}F-FB-tenascin-C aptamer at indicated time points. White arrow indicates tumor. (C) Representative coronal PET images of mice bearing subcutaneous H460 xenograft injected with ^{18}F-FB-tenascin-C aptamer at 30 min and 1 and 2 h after injection. White arrow indicates site of tumor. (D) Comparison between ^{18}F-FB-tenascin-C aptamer and ^{18}F-FB-Sc aptamer in tumor uptake at different time points (0.5, 1, and 2 h after injection) (n = 4/group). *Significance between aptamer and Sc aptamer tumor uptake.

Statistical Analysis

Results were presented as mean ± SD. Group comparisons were made using the Student t test for unpaired data. P values of less than 0.05 were considered statistically significant.

RESULTS

Synthesis and Labeling of Aptamers

The aptamers, which have different folding structures based on minimal energy calculation (Fig. 1), were modified to have a 6-carbon chain and only 1 primary amine group at the 5′-position for conjugation purposes (Fig. 2). The conjugation of ^{18}F-SFB to aptamer was conducted in basic sodium phosphate buffer (Fig. 2) and resulted in less than 2% conversion as detected by HPLC.

TABLE 1
Biodistribution of ^{18}F-FB-Tenascin-C Aptamer at 0.5, 1, and 2 Hours After Injection (%ID/g, $n = 4$)

Organ	0.5 h	1 h	2 h
Gallbladder	1.53 ± 0.46	2.08 ± 0.85	1.17 ± 0.24
Liver	4.54 ± 0.87	0.62 ± 0.06	0.21 ± 0.04
Kidneys	48.98 ± 33.29	3.84 ± 0.48	1.12 ± 0.47
Tumor	0.97 ± 0.19	0.52 ± 0.08	0.42 ± 0.16
Muscle	0.31 ± 0.04	0.19 ± 0.01	0.08 ± 0.04
Blood	1.20 ± 0.24	0.3 ± 0.05	0.07 ± 0.01

The purification of ^{18}F-FB aptamer was achieved using a NAP-5 column. Using this purification method, we obtained ^{18}F-FB aptamer as a mixture with its nonlabeled form. The average radiochemical yield was 1.47% ± 0.16% (non–decay-corrected, $n = 4$), calculated from ^{18}F-SFB, with a specific activity of 3.75–5.36 GBq/μmol (101.4–145 mCi/μmol). Similar to SFB conjugation, reaction of aptamer with *p*-SCN-Bn-NOTA resulted in a low conjugation yield, and most of the aptamer remained without chelator attached, as confirmed by liquid chromatography–mass spectrometric analysis. Labeling with ^{64}Cu was more straightforward using ^{64}Cu-acetate (Fig. 2) and resulted in higher radiochemical yields (32% ± 3%, non–decay-corrected, $n = 4$), calculated from the start of synthesis to the elution of the labeled aptamer from the NAP-5 column. The specific activities of ^{64}Cu-NOTA aptamer were higher, with values ranging from 16.09 to 18.76 GBq/μmol (435–507.2 mCi/μmol).

Aptamer Stability In Vitro and In Vivo

To evaluate the stability of the aptamers, they were incubated in mouse serum for 1 h at 37°C and thereafter loaded on agarose gel and compared with aptamers incubated in PBS. No significant degradation of the aptamers was observed (Fig. 3A). Possible demetallation of ^{64}Cu-NOTA aptamers was first evaluated in vitro by incubation in PBS and then mouse serum for different time periods. A negligible amount of free copper was detected up to 24 h using radio-TLC (Supplemental Figs. 1 and 2). Demetallation of ^{64}Cu-NOTA-tenascin-C aptamer was further evaluated in vivo in mouse blood and urine at several time points after intravenous injection (Figs. 3B and 3C). The blood and urine aliquots were compared against free ^{64}Cu. The labeled aptamer had an R_f of 0.9, whereas free ^{64}Cu stayed at the original spot (Figs. 3B and 3C). No free ^{64}Cu was detected in the blood and urine at all the time points examined (Figs. 3B and 3C).

Evaluation of Labeled Aptamer as Imaging Agent in Tumor Xenografts

In vitro evaluation of tenascin-C expression by different tumor types was done by immunofluorescence staining of tumor sections. The sections were made from mouse xenografts, generated by subcutaneous injection of U87MG glioma cells and H460 lung cancer cells, and orthotopic injection of MDA-MB-435 breast cancer cells into the mammary gland. Staining with anti–tenascin-C antibody clearly showed that both U87MG and MDA-MB-435 tumors were positive and stained similarly for tenascin-C expression, whereas H460 tumor was negative. Additional staining was also done using FITC-labeled aptamer on frozen sections from the above-mentioned xenografts and showed results similar to those of the antibody (Fig. 4A).

The initial PET studies were performed with ^{18}F-FB-tenascin-C aptamer using mice with U87MG (tenascin-C–positive) and H460 (tenascin-C–negative) tumors (Figs. 4B and 4C). ^{18}F-FB-tenascin-C aptamer PET clearly visualized tenascin-C–positive tumors but not tenascin-C–negative tumors (Figs. 4B and 4C). At 30 min after injection, ^{18}F-FB-tenascin-C aptamer had modest accumulation (0.97 ± 0.19 %ID/g, Table 1) in the positive tumor, with low tumor-to-blood (T/B) ratio (0.83 ± 0.23, Table 2) and moderate tumor-to-muscle (T/M) ratio (3.94 ± 1.43, Table 2). In addition, at

TABLE 2
T/B and T/M Ratios of ^{18}F-FB-Tenascin-C Aptamer Over Time ($n = 4$)

Ratio	0.5 h	1 h	2 h
T/B	0.83 ± 0.23	2.06 ± 0.03	4.40 ± 0.81
T/M	3.94 ± 1.43	3.05 ± 0.27	5.16 ± 0.93

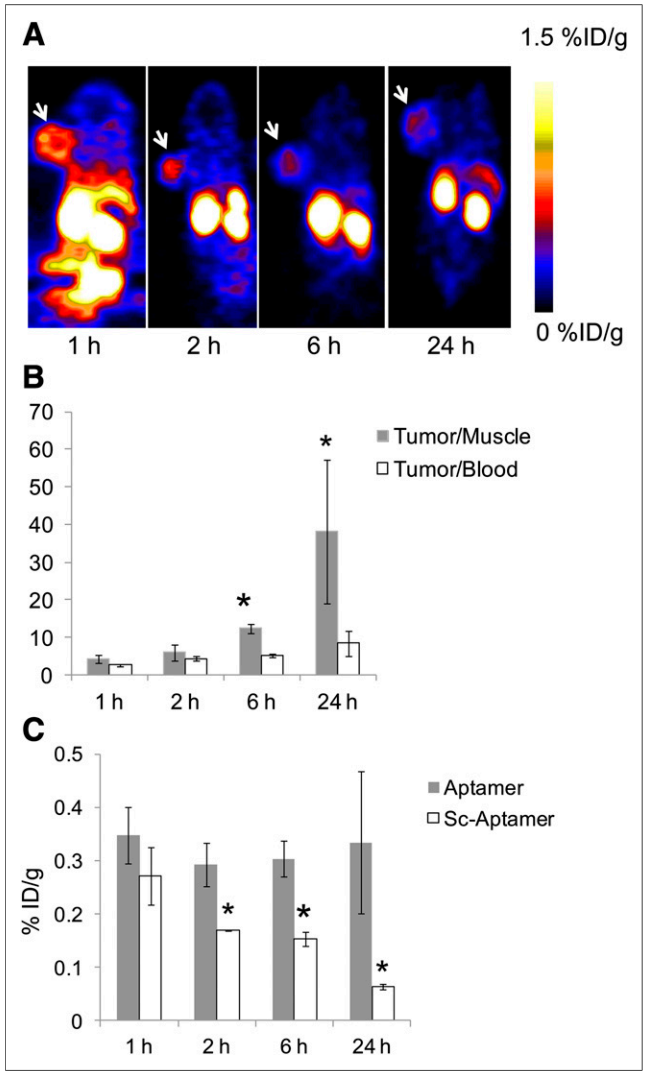

FIGURE 5. (A) Representative coronal PET images of mice at 1, 2, 6, and 24 h after injection of ^{64}Cu-NOTA-tenascin-C aptamer. White arrow indicates tumor. (B) T/M and T/B ratios of ^{64}Cu-NOTA-tenascin-C aptamer over time. Results are presented as average of 5 mice ± SD. *Significance between 6 and 24 h and 1 and 2 h. (C) Comparison of tumor uptake between ^{64}Cu-NOTA-tenascin-C aptamer and ^{64}Cu-NOTA-Sc aptamer ($n = 5$/group). *Significance between aptamer and Sc aptamer tumor uptake.

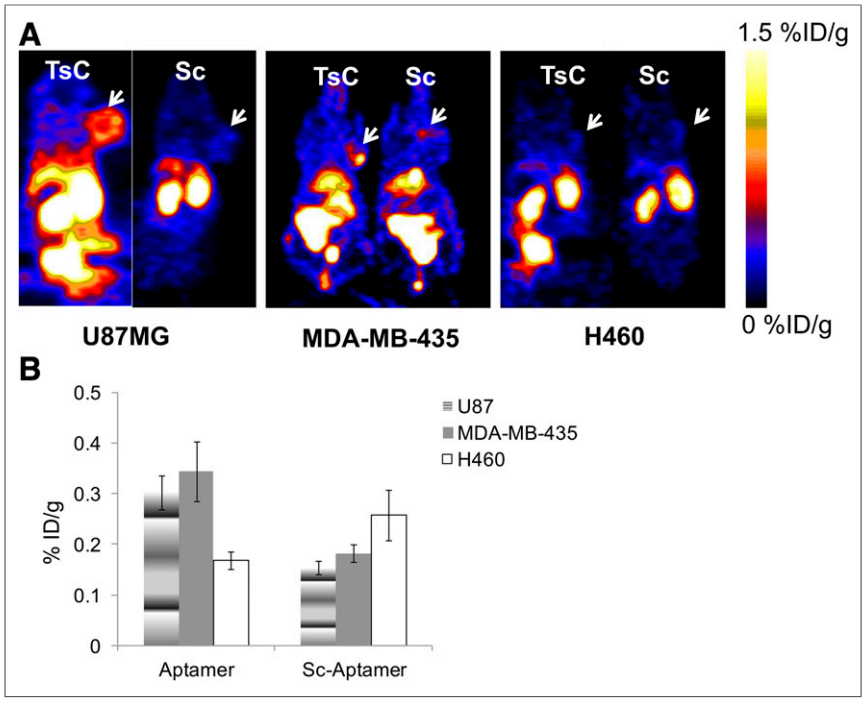

FIGURE 6. (A) Representative coronal PET images of ^{64}Cu-NOTA-tenascin-C aptamer and ^{64}Cu-NOTA-Sc aptamer in different tumor models (tenascin-C–positive [U87MG and MDA-MB-435] and tenascin-C–negative [H460]) at 6 h after injection. White arrows represent tumor location. (B) Quantified results of tumor uptake of both tracers, calculated from PET images at 6 h after injection (n = 5/group). TsC = tenascin-C.

30 min after injection, ^{18}F-FB-tenascin-C aptamer showed a high accumulation in the kidneys (49 ± 33.3 %ID/g, Table 1), moderate uptake in the liver (4.5 ± 0.87 %ID/g), and some uptake in the gallbladder (1.5 ± 0.46 %ID/g) and the blood (1.2 ± 0.24 %ID/g). At 1 h after injection, the uptake in the kidneys decreased to 3.84 ± 0.49 %ID/g along with further reduced uptake in the liver, gallbladder, and blood (Table 1), resulting in higher imaging contrast and T/B ratio (2.06 ± 0.03; Fig. 4B; Table 2). The uptake in these organs continued to decrease over time and at 2 h after injection was less than 50% of the initial uptake (Table 1). ^{18}F-FB-tenascin-C aptamer uptake in the positive tumor decreased to 0.52 ± 0.1 %ID/g at 1 h after injection, which may be due to the clearance of the radiolabeled aptamer or its possible metabolites from the blood, and remained almost the same at the 2-h time point, at which the T/B and T/M ratios increased slightly (4.40 ± 0.81 and 5.17 ± 0.93, respectively, Table 2). The comparison of tumor uptake between ^{18}F-FB-tenascin-C aptamer and ^{18}F-FB-Sc aptamer showed significant differences at all the time points examined, with ^{18}F-FB-tenascin-C aptamer having a much higher tumor uptake than ^{18}F-FB-Sc aptamer (Fig. 4D). To verify the uptake in various organs and the specificity of the aptamer, biodistribution and blocking studies were performed. Biodistribution results correlated with PET images and showed uptake in the liver, kidneys, and tumor (Supplemental Fig. 3). No significant uptake was found in the long bones, suggesting that no defluorination occurred. Blocking studies with a 100-fold excess of specific aptamer eliminated the accumulation of the labeled aptamer in the tumor. These experiments also showed a more rapid clearance of the activity from the metabolic organs.

To image at later time points and increase the T/B and T/M ratios, tenascin-C aptamer and Sc aptamer were labeled with ^{64}Cu, which has a half-life of 12.7 h. Similarly to ^{18}F, ^{64}Cu-NOTA-tenascin-C aptamer clearly visualized tenascin-C–positive U87MG tumors at all time points, up to 24 h after injection (Fig. 5A). T/M ratios increased significantly at 6 and 24 h after injection (Fig. 5B). T/B ratios were also elevated at later time points but not as drastically as the T/M ratios (Fig. 5B). Similarly to ^{18}F-FB-tenascin-C aptamer, ^{64}Cu-NOTA-tenascin-C aptamer had low accumulation in nonspecific organs, such as the kidneys and liver, at 1 h after injection (Supplemental Fig. 4). ^{64}Cu-NOTA-Sc aptamer showed relatively faster clearance from the tumor and nonspecific specific organs than ^{64}Cu-NOTA-tenascin-C aptamer (Fig. 5C; Supplemental Fig. 4).

Further comparison between ^{64}Cu-NOTA-tenascin-C aptamer and ^{64}Cu-NOTA-Sc aptamer was done in tenascin-C–positive tumor (MDA-MB-435) and tenascin-C–negative tumor (H460, Figs. 6A and 6B). Although ^{64}Cu-NOTA-Sc aptamer had similar uptake between tenascin-C–positive and –negative tumors (Fig. 6B), ^{64}Cu-NOTA-tenascin-C aptamer had significantly higher uptake in tenascin-C–positive models than ^{64}Cu-NOTA-Sc aptamer (Figs. 6A and 6B).

DISCUSSION

The extracellular matrix protein tenascin-C is transiently expressed in pathologies such as tissue injury and inflammation; however, in the tumor microenvironment tenascin-C is constantly expressed (*6,7*). The role of tenascin-C seems to be somewhat different with dependence on tumor type, perhaps because of its ability to bind and interact with multiple cytokines, integrins, and growth factors (*5,8*). Tenascin-C is expressed and secreted by stroma in most solid tumors, and it plays a role in multiple oncogenesis pathways including invasion, angiogenesis, enhancement of proliferation, and metastasis formation (*6*).

Few attempts to image tumor tenascin-C expression have been reported (*16,24*). Heuveling et al. described a phase 0 clinical trial of anti–tenascin-C minibody, labeled with ^{124}I (*24*). At 30 min after injection, the tumor was detected only in 1 patient of 4. In addition, at 24 h after injection the amount of radioactivity in the blood pool (4–5 %ID/g) was similar to the amount in the tumor and resulted in low tumor-to-background signal (*24*). Another study described in vivo evaluation of an RNA aptamer (TTA1) labeled with SPECT isotope ^{99m}Tc (*16*). The tumor-to-background signal was low at early time points but significantly improved by 18 h after injection, a time point at which there was clear visualization of the tenascin-C–positive tumor (*16*). However, at that time point, the absolute uptake in the tumor was about 1 %ID/g, similar to that of ^{18}F-FB-tenascin-C aptamer at 30 min after injection. Unfortunately, SPECT does not allow quantification of protein levels and gives only qualitative results. Together with the relatively low accumulation of the tracer in the tumor tissue, it might prove insufficient for differentiating tenascin-C–positive from tenascin-C–negative tumors in human patients.

In this study, we applied direct labeling of tenascin-C DNA aptamer with PET isotopes ^{18}F and ^{64}Cu. The conjugation to ^{18}F-SFB prosthetic group or to NOTA chelator resulted in a low but usable

yield. We hypothesized that the 3-dimensional structure of aptamers might have created steric interference for the single primary amine, and therefore the amine was not reactive enough for conjugation. Shortening the length of the aptamer for future labeling and imaging application may be essential. It has been recently shown that free ^{64}Cu accumulates in xenograft tumors (*25*). We addressed this issue by labeling the aptamer with ^{64}Cu and validating that there is no free copper in the blood and urine. Moreover, similar behavior of tenascin-C aptamer labeled with either ^{18}F or ^{64}Cu confirms negligible transchelation of ^{64}Cu-labeled NOTA aptamer conjugate.

FITC-labeled tenascin-C aptamer was compared with an anti–tenascin-C antibody in vitro using tumor sections and showed similar staining (Fig. 4A). In vivo PET imaging studies showed that labeled tenascin-C aptamer can clearly visualize tenascin-C–positive but not –negative tumors (Fig. 6A). It seems that tenascin-C aptamer does not accumulate in the tumor after initial binding, probably because of its rapid clearance, hence labeling with short-half-lived isotopes such as ^{18}F is sufficient for PET imaging application. The rapid clearance of the DNA tenascin-C aptamer can be one of the reasons that the absolute uptake of the aptamer in the tumor is relatively low. On the other hand, rapid clearance also makes the aptamer less probable to undergo degradation in vivo by DNase. Another possible reason for relatively low tumor uptake is that the target is extracellular and the probe is not internalized or trapped inside cells. Similarly, ^{64}Cu cannot be trapped inside the cells by transchelation. The comparable tumor uptake of the aptamer labeled with either ^{18}F or ^{64}Cu supports this reasoning.

Another advantage of tenascin-C aptamer is its low accumulation in nonspecific organs (i.e., liver and kidneys) as early as 1 h after injection, leading to high tumor-to-background ratios. Of special importance is the liver, which is a target of many types of metastases and has relatively high nonspecific accumulation of different PET tracers (*26,27*). Tenascin-C aptamer has almost no accumulation in the liver, which makes it useful for imaging liver metastases. Relatively high accumulation of the tracer in the kidneys at early time points might be related to the negatively charged phosphodiester groups of the oligonucleotide.

CONCLUSION

Aptamers seem to be a promising platform for developing PET imaging agents. Tenascin-C aptamer, labeled with ^{18}F or ^{64}Cu, demonstrated appropriate properties of tumor contrast that suggest utility for clinical evaluation of tenascin-C expression. Nevertheless, ^{18}F labeling requires better yield for clinical translation. The knowledge of tenascin-C expression may help clinicians select and monitor appropriate therapies, including future anti–tenascin-C therapies.

DISCLOSURE

The costs of publication of this article were defrayed in part by the payment of page charges. Therefore, and solely to indicate this fact, this article is hereby marked "advertisement" in accordance with 18 USC section 1734. This work was supported by an intramural research program of the National Institute of Biomedical Imaging and Bioengineering (NIBIB), National Institutes of Health (NIH), National Basic Research Program of China (2014CB744503, 2013CB733802, 2015CB931800, and 2015CB931803); National Natural Science Foundation of China (81371596, 81130028, and 31210103913); Key Grant Project of Heilongjiang Province (GA12C302); PhD Programs Foundation of Ministry of Education of China (201123071100203); and the Key Laboratory of Molecular Imaging Foundation (College of Heilongjiang Province). No other potential conflict of interest relevant to this article was reported.

REFERENCES

1. Chiquet-Ehrismann R, Mackie EJ, Pearson CA, Sakakura T. Tenascin: an extracellular matrix protein involved in tissue interactions during fetal development and oncogenesis. *Cell.* 1986;47:131–139.
2. Chiquet-Ehrismann R, Chiquet M. Tenascins: regulation and putative functions during pathological stress. *J Pathol.* 2003;200:488–499.
3. Tanaka R, Seki Y, Saito Y, et al. Tenascin-C-derived peptide TNIIIA2 highly enhances cell survival and PDGF-dependent cell proliferation through potentiated and sustained activation of integrin α5β1. *J Biol Chem.* 2014;289:17699–17708.
4. Tastekin D, Tas F, Karabulut S, et al. Clinical significance of serum tenascin-C levels in breast cancer. *Tumour Biol.* 2014;35:6619–6625.
5. Midwood KS, Hussenet T, Langlois B, Orend G. Advances in tenascin-C biology. *Cell Mol Life Sci.* 2011;68:3175–3199.
6. Midwood KS, Orend G. The role of tenascin-C in tissue injury and tumorigenesis. *J Cell Commun Signal.* 2009;3:287–310.
7. Oskarsson T, Acharyya S, Zhang XH, et al. Breast cancer cells produce tenascin C as a metastatic niche component to colonize the lungs. *Nat Med.* 2011;17:867–874.
8. Orend G, Chiquet-Ehrismann R. Tenascin-C induced signaling in cancer. *Cancer Lett.* 2006;244:143–163.
9. Leins A, Riva P, Lindstedt R, Davidoff MS, Mehraein P, Weis S. Expression of tenascin-C in various human brain tumors and its relevance for survival in patients with astrocytoma. *Cancer.* 2003;98:2430–2439.
10. Orend G. Potential oncogenic action of tenascin-C in tumorigenesis. *Int J Biochem Cell Biol.* 2005;37:1066–1083.
11. Rolle K, Nowak S, Wyszko E, et al. Promising human brain tumors therapy with interference RNA intervention (iRNAi). *Cancer Biol Ther.* 2010;9:396–406.
12. Zalutsky MR, Reardon DA, Akabani G, et al. Clinical experience with alpha-particle emitting ^{211}At: treatment of recurrent brain tumor patients with ^{211}At-labeled chimeric antitenascin monoclonal antibody 81C6. *J Nucl Med.* 2008; 49:30–38.
13. Reardon DA, Zalutsky MR, Akabani G, et al. A pilot study: ^{131}I-antitenascin monoclonal antibody 81C6 to deliver a 44-Gy resection cavity boost. *Neuro-oncol.* 2008;10:182–189.
14. Aloj L, D'Ambrosio L, Aurilio M, et al. Radioimmunotherapy with Tenarad, a ^{131}I-labelled antibody fragment targeting the extra-domain A1 of tenascin-C, in patients with refractory Hodgkin's lymphoma. *Eur J Nucl Med Mol Imaging.* 2014;41:867–877.
15. Schmidt KS, Borkowski S, Kurreck J, et al. Application of locked nucleic acids to improve aptamer *in vivo* stability and targeting function. *Nucleic Acids Res.* 2004;32:5757–5765.
16. Hicke BJ, Stephens AW, Gould T, et al. Tumor targeting by an aptamer. *J Nucl Med.* 2006;47:668–678.
17. Ni X, Castanares M, Mukherjee A, Lupold SE. Nucleic acid aptamers: clinical applications and promising new horizons. *Curr Med Chem.* 2011;18:4206–4214.
18. Tan W, Donovan MJ, Jiang J. Aptamers from cell-based selection for bioanalytical applications. *Chem Rev.* 2013;113:2842–2862.
19. Huang YF, Shangguan D, Liu H, et al. Molecular assembly of an aptamer-drug conjugate for targeted drug delivery to tumor cells. *ChemBioChem.* 2009;10: 862–868.
20. Daniels DA, Chen H, Hicke BJ, Swiderek KM, Gold L. A tenascin-C aptamer identified by tumor cell SELEX: systematic evolution of ligands by exponential enrichment. *Proc Natl Acad Sci USA.* 2003;100:15416–15421.
21. Reuter JS, Mathews DH. RNAstructure: software for RNA secondary structure prediction and analysis. *BMC Bioinformatics.* 2010;11:129–138.
22. *Guide for the Care and Use of Laboratory Animals.* Washington, DC: National Academy Press; 1996.
23. Jacobson O, Weiss ID, Kiesewetter DO, Farber JM, Chen X. PET of tumor CXCR4 expression with 4-^{18}F-T140. *J Nucl Med.* 2010;51:1796–1804.
24. Heuveling DA, de Bree R, Vugts DJ, et al. Phase 0 microdosing PET study using the human mini antibody F16SIP in head and neck cancer patients. *J Nucl Med.* 2013;54:397–401.
25. Kim KI, Jang SJ, Park JH, et al. Detection of increased ^{64}Cu uptake by human copper transporter 1 gene overexpression using PET with $^{64}CuCl_2$ in human breast cancer xenograft model. *J Nucl Med.* 2014;55:1692–1698.
26. Muralidharan V, Nguyen L, Banting J, Christophi C. The prognostic significance of lymphatics in colorectal liver metastases. *HPB Surg.* 2014;2014: 954604.
27. Akgül Ö, Cetinkaya E, Ersoz S, Tez M. Role of surgery in colorectal cancer liver metastases. *World J Gastroenterol.* 2014;20:6113–6122.